Passivity-Based Plug-and-Play Voltage and Frequency Control in Islanded Inverter-Based AC Microgrids

Felix Strehle, Albertus Johannes Malan, Stefan Krebs, Sören Hohmann

Abstract— In this paper, we propose a decentralized scalable, plug-and-play control of voltage-source inverters (VSIs) in islanded, inverter-based AC microgrids at primary level. Particularly in islanded mode without inertia from conventional generators in the main grid, voltage and frequency stabilization must be performed exclusively by these VSIs. In contrast to existing approaches, we propose a systematic procedure that does not require the proposition of a Lyapunov function as well as avoids computationally expensive and possibly infeasible numerical optimization. It follows passivity techniques, namely *interconnection and damping assignment passivity-based control (IDA-PBC)* on the basis of *port-Hamiltonian systems (PHSs)* theory. By employing the Hamiltonian naturally obtained from the PHS approach as Lyapunov function and analyzing load dynamics, we prove microgrid-wide asymptotic voltage and frequency stability. A simulation validating our theoretical results concludes our work.

I. INTRODUCTION

Inverter-based AC microgrids have been identified as a key element of future electrical energy supply systems [1][2][3]. They provide a systemic approach to cope with the rising integration of flexible loads, and intermittent renewable energy sources and storage devices summarized as *distributed generation units (DGUs)*, at distribution (medium and low voltage) level. These DGUs commonly operate in DC and thus interface with the remaining AC microgrid via DC-AC inverters comprising controllable VSIs and RLC filters (see Fig. 2) [1][2][3].

Among the manifold control challenges in inverter-based microgrids, reliable operation in *islanded* mode represents one of the most demanding scenarios. In absence of the stabilizing effect of conventional generators in the main grid, ancillary services, predominantly comprising voltage and frequency stabilization, must be performed exclusively by local VSI controllers at primary level to ensure proper active and reactive power flows [3][4]. A further challenge of integrating a high share of DGUs is their varying availability due to the intermittent nature of most renewable energy sources, which can in worst case lead to plug-in and -out operations [5].

Thus, primary level control design for microgrids with multiple interacting DGUs focuses on decentralized methods (cf. Fig. 2 [6]). Decentralized control approaches only rely on local DGU information and measurements

for the corresponding local VSI control design which (i) makes them independent of the overall microgrid size and thus *scalable*; (ii) drastically simplifies the control design by decomposing the microgrid into more manageable, modular subsystems; (iii) allows for the addition or removal of DGU units in a *plug-and-play* fashion without requiring changes to any existing local controllers.

The most common decentralized control approaches are based on conventional droop control and extensions thereof (see for example [3][4][7]). Their main issues are load-dependent voltage and frequency deviations, propagation of voltage errors along resistive lines, and poor performance at distribution level, where a low X/R ratio results in a non-negligible coupling of active and reactive power. Thus, droop-based methods necessitate a secondary control layer, along with some form of communication, to guarantee offset-free stabilization of voltages and frequency [3][4]. Alternative decentralized, plug-and-play control approaches are based on the concept of neutral interactions which give control laws via numerical optimization [5][8][9][10]. However, they require information about the lines connected to each DGU and they obtain control gains from linear matrix inequalities which are not always numerically feasible. In [11], a line-independent extension of [8] is proposed using a classical Lyapunov function approach which, however, necessitates solving an even more cumbersome optimization problem. This leads to [12] whose control design for DC microgrids avoids numerical optimization entirely by employing passivity theory and exploiting its link to Lyapunov stability (cf. [13, pp. 40]). However, heuristically proposing a suitable Lyapunov function remains a significant stumbling block.

In this work, we circumvent the proposition of a Lyapunov function while still employing passivity theory and exploiting its link to Lyapunov stability by following an *IDA-PBC* approach based on *PHSs*. For the voltage and frequency control of single VSIs, comprehensive IDA-PBC designs have been proposed for example in [14][15][16]. In contrast to these works, we extend our perspective to an AC microgrid level and propose a new design for an IDA passivity-based voltage and frequency control law for DGU VSI interfaces. The resulting proportional controller achieves asymptotic voltage and frequency stability at each DGU under inequality conditions. These conditions are obtained by analyzing the closed-loop system subject to ZP load dynamics. By employing the modularity of passive systems and using the

F. Strehle, A. J. Malan, S. Krebs, S. Hohmann are with the Institute of Control Systems, Karlsruhe Institute of Technology (KIT), 76131, Karlsruhe, Germany `felix.strehle@kit.edu`

Hamiltonian naturally obtained from the PHS approach as a Lyapunov function, we prove global asymptotic voltage and frequency stability for the whole microgrid.

In summary, our main contributions comprise (i) the proposition of a scalable, plug-and-play voltage and frequency control law for inverter-based AC microgrids, which directly delivers (ii) a Lyapunov function allowing for a subsequent proof of global asymptotic voltage and frequency stability.

II. BASIC PROCEDURE AND FUNDAMENTALS

In the first part of the paper (Section III), we formulate the subsystems *DGU* and *electrical line* comprising any AC microgrid as port-Hamiltonian dynamics of the form

$$\dot{\boldsymbol{x}} = [\boldsymbol{J}(\boldsymbol{x}) - \boldsymbol{R}(\boldsymbol{x})] \frac{\partial H(\boldsymbol{x})}{\partial \boldsymbol{x}} + \boldsymbol{g}(\boldsymbol{x})\boldsymbol{u} + \boldsymbol{k}(\boldsymbol{x})\boldsymbol{d} \quad (1)$$

where $\boldsymbol{x} \in \mathbb{R}^n$ is the state vector, $\boldsymbol{u} \in \mathbb{R}^m$ is the control input vector, $\boldsymbol{d} \in \mathbb{R}^d$ is the disturbance vector [17, p. 69]. The conjugated outputs are omitted in the models as they will not be necessary for the following design. Note that they do not necessarily correspond to measurements, but are simply power-conjugated variables to $\boldsymbol{u}$ and $\boldsymbol{d}$. $\boldsymbol{J}(\boldsymbol{x})$, $\boldsymbol{R}(\boldsymbol{x})$, $\boldsymbol{g}(\boldsymbol{x})$, and $\boldsymbol{k}(\boldsymbol{x})$ are real-valued matrices of respective sizes with $\boldsymbol{J}(\boldsymbol{x}) = -\boldsymbol{J}^\mathsf{T}(\boldsymbol{x})$ and $\boldsymbol{R}(\boldsymbol{x}) = \boldsymbol{R}^\mathsf{T}(\boldsymbol{x}) \succeq 0$ (positive semidefinite). The Hamiltonian $H(\boldsymbol{x}) : \mathbb{R}^n \to \mathbb{R}$ is a smooth function of the states representing the total stored energy in the system. Its minimum represents the equilibrium $\boldsymbol{x}^*$ of the system.

Remark 1: Equilibrium variables will be denoted by *.

In the second part of the paper (Section IV), we formulate an IDA-PBC for a general VSI interface following the approach detailed in [18] to achieve stability of the voltage and frequency setpoints. Initially, the undisturbed dynamics in (1), i.e. $\boldsymbol{d} = \boldsymbol{0}$, are split into actuated (α) and unactuated (ν) parts

$$\begin{bmatrix} \dot{\boldsymbol{x}}_\alpha \\ \dot{\boldsymbol{x}}_\nu \end{bmatrix} = \begin{bmatrix} \boldsymbol{f}_\alpha(\boldsymbol{x}) \\ \boldsymbol{f}_\nu(\boldsymbol{x}) \end{bmatrix} + \begin{bmatrix} \boldsymbol{G}_\alpha(\boldsymbol{x}) \\ \boldsymbol{0}_{(n-m)\times m} \end{bmatrix} \boldsymbol{u}, \quad (2)$$

using a suitable transformation. The matrix $\boldsymbol{G}_\alpha(\boldsymbol{x})$ is a square matrix of size $(m \times m)$. Then, in order to solve the IDA-PBC matching equation (cf. (3) [19]) for the desired Hamiltonian $H_c(\boldsymbol{x})$, design parameters are chosen to be state-independent

$$\boldsymbol{F}_c := \boldsymbol{J}_c - \boldsymbol{R}_c = \begin{bmatrix} \boldsymbol{F}_\alpha \\ \boldsymbol{F}_\nu \end{bmatrix}, \quad (3)$$

with the natural choice for the full-rank left annihilator

$$\boldsymbol{G}^\perp = \begin{bmatrix} \boldsymbol{0}_{(n-m)\times m} & \boldsymbol{I}_{(n-m)\times(n-m)} \end{bmatrix}. \quad (4)$$

Remark 2: Functions and matrices of the desired *closed-loop* system are denoted with the subscript c. With (3) and (4), the matching equation (cf. (3) [19]) can be simplified to the linear system of first-order PDEs

$$\boldsymbol{F}_\nu \frac{\partial H_c(\boldsymbol{x})}{\partial \boldsymbol{x}} \overset{!}{=} \boldsymbol{f}_\nu(\boldsymbol{x}), \quad (5)$$

dependent on the desired Hamiltonian H_c. Solving (5) for all $\boldsymbol{x}$ is possible if and only if

$$\frac{\partial f_{\nu,k}(\boldsymbol{x})}{\partial \boldsymbol{x}} \boldsymbol{\nu}_l - \frac{\partial f_{\nu,l}(\boldsymbol{x})}{\partial \boldsymbol{x}} \boldsymbol{\nu}_k \overset{!}{=} 0, \quad k, l = 1 \ldots n - m, \quad (6)$$

which will yield restrictions on the control design. The IDA-PBC law for the transformed α-ν-system in (2) is then given by

$$\boldsymbol{u}(\boldsymbol{x}) = \boldsymbol{G}_\alpha^{-1} \left[\boldsymbol{F}_\alpha \frac{\partial H_c(\boldsymbol{x})}{\partial \boldsymbol{x}} - \boldsymbol{f}_\alpha(\boldsymbol{x}) \right]. \quad (7)$$

For a later stability analysis, we establish the following lemma:

Lemma 1: If $\boldsymbol{Q} \succ 0$ and $\boldsymbol{R}(\boldsymbol{x}) = \boldsymbol{R}^\mathsf{T}(\boldsymbol{x}) \succ 0$ (positive definite), then a PHS (1) with quadratic Hamiltonian $H(\boldsymbol{x}) = \frac{1}{2}\boldsymbol{x}^\mathsf{T}\boldsymbol{Q}\boldsymbol{x}$ is strictly passive and globally asymptotically stable in the equilibrium $\boldsymbol{x}^* = \arg\min_{\boldsymbol{x}} H(\boldsymbol{x})$, with $H(\boldsymbol{x})$ used as a Lyapunov function.

Proof: (a) If $\boldsymbol{Q} \succ 0$, then $H(\boldsymbol{x})$ is a positive definite function (cf. [20, p. 117]) with a minimum at $\boldsymbol{x}^*$ such that $H(\boldsymbol{x}^*) = 0$ and $H(\boldsymbol{x}) > 0$ for all $\boldsymbol{x} \neq \boldsymbol{x}^*$. (b) Furthermore, with $\boldsymbol{R}(\boldsymbol{x}) \succ 0$ we can show

$$\frac{\mathrm{d}H(\boldsymbol{x})}{\mathrm{d}t} = \frac{\partial^\mathsf{T} H(\boldsymbol{x})}{\partial \boldsymbol{x}} \dot{\boldsymbol{x}} \quad (8)$$

$$= -\frac{\partial^\mathsf{T} H(\boldsymbol{x})}{\partial \boldsymbol{x}} \boldsymbol{R}(\boldsymbol{x}) \frac{\partial H(\boldsymbol{x})}{\partial \boldsymbol{x}} < 0 \quad \forall \boldsymbol{x} \neq \boldsymbol{x}^*. \quad (9)$$

The strict passivity of (1) follows from (a) and (b) [20, p. 236] where $H(\boldsymbol{x})$ is a Lyapunov function. The radially unbounded and positive definite nature of $H(\boldsymbol{x})$ at $\boldsymbol{x}^*$ and strict passivity ensure the global asymptotic stability of the equilibrium $\boldsymbol{x}^*$ of (1) for $\boldsymbol{u} \equiv 0$, $\boldsymbol{d} \equiv 0$ via Lyapunov's direct method [21, pp. 44–45]. ∎

III. MODELING

Section III-A introduces the islanded AC microgrid along with its subsystems and defines the framework on which the subsystem models are based. Sections III-B and III-C present PHS models of the *DGU* and *line* subsystems, respectively. Finally, the passivity and stability of the islanded microgrid is discussed in Section III-D.

A. System description

We consider an islanded AC microgrid comprising DGUs, lines and loads in the *dq* reference frame rotating at $\omega_0 = 2\pi\,50\,\text{Hz}$. The zero-sequence is neglected by assuming a balanced network as in [11]. Furthermore, a *load-connected* topology is considered in which loads are mapped to the DGU terminals, denoted as the *Point of Common Coupling* (PCC), via Kron Reduction as in [5][8][10][11]. The DGUs are connected by π-model electrical lines to form a bipartite graph as in Fig. 1, a single connection of which is illustrated in Fig. 2. Note that a DGU may connect to multiple lines.

Remark 3: The subscripts d and q denote the respective components of a variable in the *dq* coordinate frame. The subscript *dq* denotes a vector of the d and q components, i.e. $\boldsymbol{V}_{dq} := [V_d, V_q]^\mathsf{T}$.
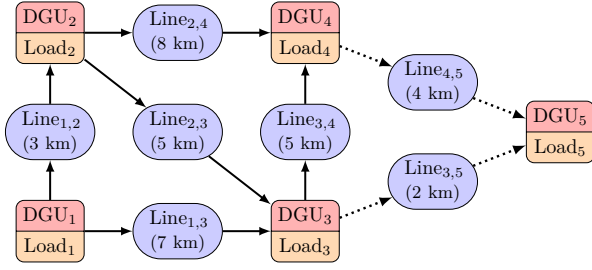
Fig. 1. Bipartite graph representation of an islanded AC microgrid with DGUs, Kron-reduced loads associated with the respective DGUs, and lines interconnecting the various DGUs; dotted lines indicate the plug-and-play nature of the microgrid

Remark 4: Variables in the *dq* frame (rotating at frequency ω_0) can be considered Cartesian representations of phasors in polar coordinates, i.e. $V \angle \theta$. Asymptotically stable *dq* systems imply $\theta = const.$, and are therefore also asymptotically stable as phasors with the frequency of the rotating phasors $\omega = \dot{\theta} + \omega_0 = \omega_0$, since $\dot{\theta} = 0$. Asymptotic frequency stability is therefore implicitly present in an asymptotically stable *dq* system.

B. DGU Inverter Interface Model

Fig. 2 depicts a DGU circuit diagram in *dq* coordinates at a node i in the microgrid. The DC voltage source represents a renewable energy source or storage device, connected to the AC microgrid through a VSI and an RLC filter. The VSI and filter inductance losses are lumped together in R_{ti}. To simplify the control design in the sequel, we assume the DC source to be an unconstrained power source or sink [5][11] and the saturation limits of the VSI are ignored [11]. Furthermore, we model the VSI using the averaged switch modeling technique [1], since VSIs usually operate at very high frequencies compared to the microgrid frequency and the RLC filter sufficiently suppresses the VSI switching dynamics. The disturbance current results from the sum of the load and line currents, i.e. $\boldsymbol{I}_{\mathrm{Z,dq},i} = \boldsymbol{I}_{\mathrm{L,dq},i} + \boldsymbol{I}_{\mathrm{dq},ij}$. Following [16], we model a DGU at node i as port-Hamiltonian dynamics

$$\begin{bmatrix} L_{ti}\dot{I}_{\mathrm{d},i} \\ L_{ti}\dot{I}_{\mathrm{q},i} \\ C_{ti}\dot{V}_{\mathrm{d},i} \\ C_{ti}\dot{V}_{\mathrm{q},i} \end{bmatrix} = \begin{bmatrix} -R_{ti} & \omega_0 L_{ti} & -1 & 0 \\ -\omega_0 L_{ti} & -R_{ti} & 0 & -1 \\ 1 & 0 & 0 & \omega_0 C_{ti} \\ 0 & 1 & -\omega_0 C_{ti} & 0 \end{bmatrix} \begin{bmatrix} I_{\mathrm{d},i} \\ I_{\mathrm{q},i} \\ V_{\mathrm{d},i} \\ V_{\mathrm{q},i} \end{bmatrix}$$
$$+ \begin{bmatrix} 1 & 0 \\ 0 & 1 \\ 0 & 0 \\ 0 & 0 \end{bmatrix} \begin{bmatrix} V_{\mathrm{t,d},i} \\ V_{\mathrm{t,q},i} \end{bmatrix} - \begin{bmatrix} 0 & 0 \\ 0 & 0 \\ 1 & 0 \\ 0 & 1 \end{bmatrix} \begin{bmatrix} I_{\mathrm{Z,d},i} \\ I_{\mathrm{Z,q},i} \end{bmatrix}, \quad (10\mathrm{a})$$

(cf. (1)) with Hamiltonian

$$H_i(\boldsymbol{x}_i) = \frac{1}{2}\boldsymbol{x}_i^\mathsf{T} \mathrm{Diag}\left[\frac{1}{L_{ti}}, \frac{1}{L_{ti}}, \frac{1}{C_{ti}}, \frac{1}{C_{ti}}\right]\boldsymbol{x}_i, \quad (10\mathrm{b})$$

state variables $\boldsymbol{x}_i = [L_{ti}I_{\mathrm{d},i}, L_{ti}I_{\mathrm{q},i}, C_{ti}V_{\mathrm{d},i}, C_{ti}V_{\mathrm{q},i}]^\mathsf{T}$, input $\boldsymbol{u}_i = [V_{\mathrm{t,d},i}, V_{\mathrm{t,q},i}]^\mathsf{T}$, disturbance $\boldsymbol{d}_i = [I_{\mathrm{Z,d},i}, I_{\mathrm{Z,q},i}]^\mathsf{T}$,

and interconnection and damping matrices

$$\boldsymbol{J}_i = \begin{bmatrix} 0 & \omega_0 L_{ti} & -1 & 0 \\ -\omega_0 L_{ti} & 0 & 0 & -1 \\ 1 & 0 & 0 & \omega_0 C_{ti} \\ 0 & 1 & -\omega_0 C_{ti} & 0 \end{bmatrix}, \quad (10\mathrm{c})$$
$$\boldsymbol{R}_i = \mathrm{Diag}\,[\,R_{ti},\, R_{ti},\, 0,\, 0\,]\,.$$

Remark 5: Using [17, p. 107], we can analyze the voltage and frequency stability of interconnected PHSs, i.e. the microgrid, by combining the passivity properties of the individual PHSs, i.e. the DGUs and lines. The interconnection variables obtained by decomposing the overall PHS, are exogenous inputs to the individual PHSs and may thus be neglected for the stability analysis of the individual PHSs. The current $\boldsymbol{I}_{\mathrm{dq},ij}$ is such an exogenous, interconnecting input to the DGU, which we may therefore set to $\boldsymbol{I}_{\mathrm{dq},ij} = \boldsymbol{0}$ when analyzing the DGU stability. However, the load current $\boldsymbol{I}_{\mathrm{L,dq},i}$ is part of the DGU subsystem and furthermore dependent on $\boldsymbol{V}_{\mathrm{dq},i}$. Since $\dot{\boldsymbol{V}}_{\mathrm{dq},i}$ is in turn dependent on $\boldsymbol{I}_{\mathrm{L,dq},i}$, a feedback effect occurs between the dynamics of the voltage $\boldsymbol{V}_{\mathrm{dq},i}$, the controlled variable, and the load current $\boldsymbol{I}_{\mathrm{L,dq},i}$. This effect must be considered when analyzing the voltage and frequency stability of the DGU.

1) Load Model: To account for the dynamics caused by the feedback effect discussed in Remark 5, a model of the load is required. Due to space limitations, we restrict ourselves in this work to *ZP* loads [22, p. 111] comprising constant impedance (Z) and constant power (P) loads with

$$P = P_P + Z_P \left(\frac{V}{V_0}\right)^2, \; Q = P_Q + Z_Q \left(\frac{V}{V_0}\right)^2 \quad (11)$$

the respective real and reactive powers of the load. The nominal voltage amplitude of the load is V_0 and the amplitude of the voltage phasor is

$$V^2 = V_\mathrm{d}^2 + V_\mathrm{q}^2\,. \quad (12)$$

C. Electrical Line Model

Consider the π-model of the line in Fig. 2 comprising two C legs connected by an RL branch with $C_{ij}, R_{ij}, L_{ij} > 0$. As the dynamics of the C legs only depend on the PCC voltages of the DGUs they connect to, the C legs are considered part of the respective DGU subsystems. Furthermore, C legs are treated as constant Z loads (cf. (11)) to ensure the local VSI controllers are independent of these unknown parameters. Consequently, the port-Hamiltonian line dynamics in *dq* coordinates are given by the RL branch dynamics

$$\begin{bmatrix} L_{ij}\dot{I}_{\mathrm{d},ij} \\ L_{ij}\dot{I}_{\mathrm{q},ij} \end{bmatrix} = \begin{bmatrix} -R_{ij} & \omega_0 L_{ij} \\ -\omega_0 L_{ij} & -R_{ij} \end{bmatrix} \begin{bmatrix} I_{\mathrm{d},ij} \\ I_{\mathrm{q},ij} \end{bmatrix} + \begin{bmatrix} V_{\mathrm{d},i} - V_{\mathrm{d},j} \\ V_{\mathrm{q},i} - V_{\mathrm{q},j} \end{bmatrix}, \quad (13\mathrm{a})$$

with Hamiltonian

$$H_{ij}(\boldsymbol{x}_{ij}) = \frac{1}{2}\boldsymbol{x}_{ij}^\mathsf{T} \mathrm{Diag}\left[\frac{L_{ij}}{2}, \frac{L_{ij}}{2}\right]\boldsymbol{x}_{ij}, \quad (13\mathrm{b})$$
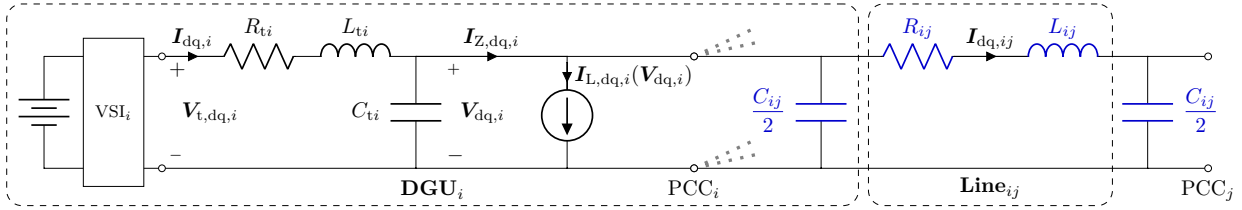
Fig. 2. Circuit diagram of a DGU comprising a VSI, a filter and a voltage-dependent current source representing a load, connected to a π-model line (blue); the legs of the line are considered part of the respective DGUs

states $\boldsymbol{x}_{ij} = [L_{ij}I_{\mathrm{d},ij}, L_{ij}I_{\mathrm{q},ij}]^\mathsf{T}$, inputs $\boldsymbol{u}_{ij} = [\boldsymbol{V}_{\mathrm{dq},i}, \boldsymbol{V}_{\mathrm{dq},j}]^\mathsf{T}$, and interconnection and damping matrices

$$\boldsymbol{J}_{ij} = \begin{bmatrix} 0 & \omega_0 L_{ij} \\ -\omega_0 L_{ij} & 0 \end{bmatrix}, \boldsymbol{R}_{ij} = \begin{bmatrix} R_{ij} & 0 \\ 0 & R_{ij} \end{bmatrix}. \quad (13c)$$

D. Microgrid Voltage and Frequency Stability

The strict passivity of the microgrid model and thus its asymptotic stability can be ascertained by analyzing the passivity of the subsystems *DGU* and *line*, and their interconnections.

Proposition 2: An islanded AC microgrid represented by a bipartite graph as in Fig. 1 consisting of π-model lines and strictly passive DGU PHSs is itself strictly passive with an asymptotically stable equilibrium given by the combined equilibria of the individual subsystems, $\boldsymbol{x}_{ij}^*$ and $\boldsymbol{x}_i^*$, respectively.

Proof: According to Lemma 1, the line PHS in (13) is strictly passive. If the DGUs, with their respective loads, are strictly passive (possibly through appropriate control), then the microgrid comprises only strictly passive subsystems interconnected by ideal flow (current) constraints which are power-conserving Dirac structures [17, p. 100]. The strict passivity of the microgrid then directly follows from [17, p. 107]. Finally, the asymptotic stability of the strictly passive microgrid is inferred from Lyapunov's direct method [21, p. 44] by using the Hamiltonian of the microgrid, i.e. the sum of the subsystem Hamiltonians, as a Lyapunov function. ∎

From Proposition 2 and Remark 4 we conclude that the voltage and frequency regulation of the microgrid reduces to controlling the local VSIs such that their corresponding DGUs are strictly passive and that their Hamiltonians have minima at the equilibria given by the desired *dq* voltage references $\boldsymbol{V}_{\mathrm{dq},i}^*$, $i = 1, \ldots, N$.

IV. FREQUENCY AND VOLTAGE CONTROL DESIGN

In Section IV-A, a voltage and frequency controller for the initially undisturbed DGU model (10), i.e. $\boldsymbol{I}_{\mathrm{Z,dq}} = \boldsymbol{0}$, is designed. The design combines *non-parameterized IDA-PBC* [19] with the systematic approach in [18]. In Section IV-B, we then analyze the robustness of the designed controller by means of the stability of the controlled DGU under disturbances $\boldsymbol{I}_{\mathrm{Z,dq}} \neq \boldsymbol{0}$.

Remark 6: For clarity in the subsequent design, the subscript i is dropped from all variables and parameters in this section, i.e. $\boldsymbol{V}_{\mathrm{dq}} := \boldsymbol{V}_{\mathrm{dq},i}$ and $R_{\mathrm{t}} := R_{\mathrm{t}i}$ etc.

A. IDA-PBC Design

Initially, the matching equation is set up (IV-A.1) and solvability restrictions are placed on the design parameters (IV-A.2). This leads to a simplified matching equation which is solved for a desired Hamiltonian establishing $\boldsymbol{V}_{\mathrm{dq}}^*$ (IV-A.3). Finally, the control law required to realize the desired system is calculated (IV-A.4).

1) Matching Equation Setup: Conveniently, the system described by (10) is for $\boldsymbol{I}_{\mathrm{Z,dq}} = \boldsymbol{0}$ already of form (2) with states $\boldsymbol{x}_\alpha = \boldsymbol{I}_{\mathrm{dq}}$ and $\boldsymbol{x}_\nu = \boldsymbol{V}_{\mathrm{dq}}$, $\boldsymbol{G}_\alpha(\boldsymbol{x}) = \boldsymbol{I}_{2\times2}$, and

$$\boldsymbol{f}_\alpha(\boldsymbol{x}) = \begin{bmatrix} -R_{\mathrm{t}}I_{\mathrm{d}} + \omega_0 L_{\mathrm{t}}I_{\mathrm{q}} - V_{\mathrm{d}} \\ -R_{\mathrm{t}}I_{\mathrm{q}} - \omega_0 L_{\mathrm{t}}I_{\mathrm{d}} - V_{\mathrm{q}} \end{bmatrix}, \quad (14a)$$

$$\boldsymbol{f}_\nu(\boldsymbol{x}) = \begin{bmatrix} I_{\mathrm{d}} + \omega_0 C_{\mathrm{t}}V_{\mathrm{q}} \\ I_{\mathrm{q}} - \omega_0 C_{\mathrm{t}}V_{\mathrm{d}} \end{bmatrix}. \quad (14b)$$

Then (6) is established with (14b) and (3), which is in this case

$$\boldsymbol{F}_{\mathrm{c}} := \boldsymbol{J}_{\mathrm{c}} - \boldsymbol{R}_{\mathrm{c}} = \begin{bmatrix} \boldsymbol{F}_\alpha \\ \boldsymbol{F}_\nu \end{bmatrix} = \begin{bmatrix} \alpha_{11} & \alpha_{12} & \alpha_{13} & \alpha_{14} \\ \alpha_{21} & \alpha_{22} & \alpha_{23} & \alpha_{24} \\ \nu_{11} & \nu_{12} & \nu_{13} & \nu_{14} \\ \nu_{21} & \nu_{22} & \nu_{23} & \nu_{24} \end{bmatrix}. \quad (15)$$

2) Design Restrictions: Evaluating the solvability requirement (6) for (10) yields

$$\nu_{12}, \nu_{13}, \nu_{21}, \nu_{24} = 0 \quad (16)$$

in (15). Port-Hamiltonian theory further requires [18]

$$\boldsymbol{R}_{\mathrm{c}} = -\frac{\boldsymbol{F}_{\mathrm{c}} + \boldsymbol{F}_{\mathrm{c}}^\mathsf{T}}{2} \overset{!}{\succeq} 0, \quad (17)$$

which restricts the available degrees of freedom to

$$\begin{aligned} \alpha_{14} &= 0, & \alpha_{12} &= -\nu_{21}, & \alpha_{11} &\leq 0, \\ \alpha_{23} &= 0, & \alpha_{13} &= -\nu_{11}, & \alpha_{22} &\leq 0, \\ \alpha_{24} &= 0, & \nu_{14} &= -\nu_{23}. \end{aligned} \quad (18)$$

With the restrictions in (16) and (18), (15) becomes

$$\boldsymbol{F}_{\mathrm{c}} = \begin{bmatrix} \alpha_{11} & -\alpha_{21} & -\nu_{11} & 0 \\ \alpha_{21} & \alpha_{22} & 0 & -\nu_{22} \\ \nu_{11} & 0 & 0 & -\nu_{23} \\ 0 & \nu_{22} & \nu_{23} & 0 \end{bmatrix} \quad (19)$$

guaranteeing that (5) is solvable and that (17) is satisfied. The matrices $\boldsymbol{J}_c$ and $\boldsymbol{R}_c$ are calculated as the skew-symmetric and symmetric parts of (19), respectively:

$$\boldsymbol{J}_c = \begin{bmatrix} 0 & -\alpha_{21} & -\nu_{11} & 0 \\ \alpha_{21} & 0 & 0 & -\nu_{22} \\ \nu_{11} & 0 & 0 & -\nu_{23} \\ 0 & \nu_{22} & \nu_{23} & 0 \end{bmatrix}, \qquad (20)$$

$$\boldsymbol{R}_c = \text{Diag}\left[-\alpha_{11}, -\alpha_{22}, 0, 0\right].$$

With (19), (5) can be written as

$$\begin{bmatrix} \nu_{11} & 0 & 0 & -\nu_{23} \\ 0 & \nu_{22} & \nu_{23} & 0 \end{bmatrix} \frac{\partial H_c(\boldsymbol{x})}{\partial \boldsymbol{x}} \overset{!}{=} \begin{bmatrix} I_d + \omega_0 C_t V_q \\ I_q - \omega_0 C_t V_d \end{bmatrix}. \qquad (21)$$

3) Desired Hamiltonian: Having simplified the matching equation (5) to (21), we now solve (21) for

$$H_c(\boldsymbol{x}) = \Psi(\boldsymbol{x}) + \Phi(\boldsymbol{x}) \qquad (22)$$

with the patricular and homogeneous solutions, $\Psi(\boldsymbol{x})$ and $\Phi(\boldsymbol{x})$, respectively. We obtain the particular solution

$$\Psi(\boldsymbol{x}) = \frac{L_t}{2\nu_{11}}\left(I_d^2 + 2\omega_0 C_t V_q I_d\right) + \frac{L_t}{2\nu_{22}}\left(I_q^2 - 2\omega_0 C_t V_d I_q\right) \qquad (23)$$

of (21) by means of computer algebra software under the restriction

$$\nu_{23} = 0. \qquad (24)$$

The choice (24) further results in a homogeneous solution of the form

$$\Phi(\boldsymbol{x}) = h(V_d, V_q), \qquad (25)$$

whose generality affords great freedom in shaping the Hamiltonian (22) such that its minimum is reached at the desired equilibrium $\boldsymbol{x}^*$, i.e.

$$\left.\frac{\partial H_c(\boldsymbol{x})}{\partial \boldsymbol{x}}\right|_{\boldsymbol{x}^*} \overset{!}{=} \boldsymbol{0}, \quad \left.\frac{\partial^2 H_c(\boldsymbol{x})}{\partial \boldsymbol{x}^2}\right|_{\boldsymbol{x}^*} \overset{!}{\succ} 0. \qquad (26)$$

Furthermore, a passive system requires that H_c be bounded from below [21, p. 116]. To this end, we choose the homogeneous solution in (25) as

$$h(V_d, V_q) = \frac{L_t}{2\nu_{11}}(\omega_0 C_t V_q)^2 + \frac{C_t}{2}(V_d - V_d^*)^2 \\ + \frac{L_t}{2\nu_{22}}(\omega_0 C_t V_d)^2 + \frac{C_t}{2}(V_q - V_q^*)^2. \qquad (27)$$

This completes the squares in (23) such that with (23) and (27), (22) becomes

$$H_c(\boldsymbol{x}) = \frac{L_t}{2\nu_{11}}\left(I_d + \omega_0 C_t V_q\right)^2 + \frac{C_t}{2}\left(V_d - V_d^*\right)^2 \\ + \frac{L_t}{2\nu_{22}}\left(I_q - \omega_0 C_t V_d\right)^2 + \frac{C_t}{2}\left(V_q - V_q^*\right)^2 \qquad (28)$$

which is quadratic. Under the condition

$$\nu_{11} > 0, \quad \nu_{22} > 0, \qquad (29)$$

H_c in (28) is convex and thus bounded from below. By further choosing the current reference

$$\begin{bmatrix} I_d^* \\ I_q^* \end{bmatrix} := \left.\begin{bmatrix} -\omega_0 C_t V_q \\ \omega_0 C_t V_d \end{bmatrix}\right|_{\boldsymbol{V}_{dq}^*} = \begin{bmatrix} -\omega_0 C_t V_q^* \\ \omega_0 C_t V_d^* \end{bmatrix} \qquad (30)$$

for the undisturbed system dependent on the voltage reference $\boldsymbol{V}_{dq}^*$, we see that H_c in (28) fulfills (26) for the equilibrium

$$\boldsymbol{x}^* = \left[L_t I_d^*, \, L_t I_q^*, \, C_t V_d^*, \, C_t V_q^*\right]^{\mathsf{T}}. \qquad (31)$$

4) Control Law: The control design is concluded by computing the IDA-PBC control law. With the design matrix (19), the desired Hamiltonian (28) and the original α-system (14a), (7) yields

$$\underset{(2\times 1)}{\boldsymbol{u}(\boldsymbol{x})} = \begin{bmatrix} R_t I_d - \omega_0 L_t I_q + \frac{\omega_0 L_t \nu_{11} - \alpha_{21}}{\nu_{22}}(I_q - \omega_0 C_t V_d) \\ +V_d - \nu_{11}(V_d - V_d^*) + \frac{\alpha_{11}}{\nu_{11}}(I_d + \omega_0 C_t V_q) \\ \hdashline R_t I_q + \omega_0 L_t I_d - \frac{\omega_0 L_t \nu_{22} - \alpha_{21}}{\nu_{11}}(I_d + \omega_0 C_t V_q) \\ +V_q - \nu_{22}(V_q - V_q^*) + \frac{\alpha_{22}}{\nu_{22}}(I_q - \omega_0 C_t V_d) \end{bmatrix}. \qquad (32)$$

To prevent undesirable coupling between the $L_t \boldsymbol{I}_{dq}$ states of the controlled system, the parameters choices

$$\nu_{22} = \nu_{11}, \quad \alpha_{21} = \omega_0 L_t \nu_{11} \qquad (33)$$

are made. With (33), the control law (32) simplifies to

$$\underset{(2\times 1)}{\boldsymbol{u}(\boldsymbol{x})} = \begin{bmatrix} R_t I_d - \omega_0 L_t I_q + V_d \\ -\nu_{11}(V_d - V_d^*) + \frac{\alpha_{11}}{\nu_{11}}(I_d + \omega_0 C_t V_q) \\ \hdashline R_t I_q + \omega_0 L_t I_d + V_q \\ -\nu_{11}(V_q - V_q^*) + \frac{\alpha_{22}}{\nu_{11}}(I_q - \omega_0 C_t V_d) \end{bmatrix}, \qquad (34)$$

where $\alpha_{11}, \alpha_{22}, \nu_{11}$ are control parameters, V_d^*, V_q^*, ω_0 are references, and the states or rather their corresponding currents and voltages V_d, V_q, I_d, I_q are measurements.

Remark 7: Considering (20), it would appear that the α_{21} choice in (33) causes a coupling of the states rather than preventing it. This counter-intuitive choice can be explained by considering the coupling present in the gradient of H_c, cf. (28).

B. Closed-Loop Voltage and Frequency Stability

In this subsection, we analyze the dynamics of the controlled DGU and set up inequalities for the control parameters and load characteristic to ensure strict passivity of the DGU subsystem as required by Proposition 2. Applying (34) to (10a) gives the controlled DGU dynamics

$$\begin{bmatrix} L_t \dot{I}_d \\ L_t \dot{I}_q \\ C_t \dot{V}_d \\ C_t \dot{V}_q \end{bmatrix} = \begin{bmatrix} -\nu_{11}(V_d - V_d^*) + \frac{\alpha_{11}}{\nu_{11}}(I_d + \omega_0 C_t V_q) \\ -\nu_{11}(V_q - V_q^*) + \frac{\alpha_{22}}{\nu_{11}}(I_q - \omega_0 C_t V_d) \\ I_d + \omega_0 C_t V_q \\ I_q - \omega_0 C_t V_d \end{bmatrix} - \begin{bmatrix} 0 \\ 0 \\ I_{Z,d} \\ I_{Z,q} \end{bmatrix}, \qquad (35)$$

in the form (1) with H_c in (28) and the $\boldsymbol{J}_c$ and $\boldsymbol{R}_c$ matrices in (20). Since the undisturbed system in (35), i.e. with $\boldsymbol{I}_{Z,dq} = 0$, is linear with the $\boldsymbol{J}_c$ and $\boldsymbol{R}_c$ matrices constant and H_c in (28) convex under (29), it also displays the shifted passivity property [21, p. 136]. From this, we may define the error

$$\boldsymbol{\epsilon} = \begin{bmatrix} \boldsymbol{\epsilon}_{\boldsymbol{I}_{dq}} \\ \boldsymbol{\epsilon}_{\boldsymbol{V}_{dq}} \end{bmatrix} := \begin{bmatrix} \boldsymbol{I}_{dq} - \boldsymbol{I}_{dq}^* \\ \boldsymbol{V}_{dq} - \boldsymbol{V}_{dq}^* \end{bmatrix} \qquad (36)$$
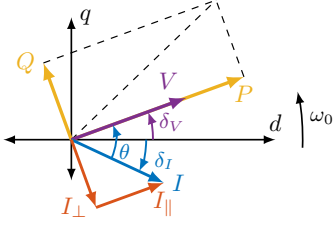
Fig. 3. Phasor diagram depicting voltage V, current I and powers P, Q in the dq frame; Measured variables are displayed in **purple**, desired variables in **blue**, intermediate variables in **red** and the load powers are in **yellow**

with $\boldsymbol{\epsilon}_{\boldsymbol{I}_{\text{dq}}} = \begin{bmatrix} \epsilon_{I_{\text{d}}}, \epsilon_{I_{\text{q}}} \end{bmatrix}^{\mathsf{T}}$ and $\boldsymbol{\epsilon}_{\boldsymbol{V}_{\text{dq}}} = \begin{bmatrix} \epsilon_{V_{\text{d}}}, \epsilon_{V_{\text{q}}} \end{bmatrix}^{\mathsf{T}}$, to obtain the error dynamics

$$\begin{bmatrix} L_{\text{t}}\dot{\epsilon}_{I_{\text{d}}} \\ L_{\text{t}}\dot{\epsilon}_{I_{\text{q}}} \\ C_{\text{t}}\dot{\epsilon}_{V_{\text{d}}} \\ C_{\text{t}}\dot{\epsilon}_{V_{\text{q}}} \end{bmatrix} = \begin{bmatrix} -\nu_{11}\epsilon_{V_{\text{d}}} + \frac{\alpha_{11}}{\nu_{11}}(\epsilon_{I_{\text{d}}} + \omega_0 C_{\text{t}}\epsilon_{V_{\text{q}}}) \\ -\nu_{11}\epsilon_{V_{\text{q}}} + \frac{\alpha_{22}}{\nu_{11}}(\epsilon_{I_{\text{q}}} - \omega_0 C_{\text{t}}\epsilon_{V_{\text{d}}}) \\ \epsilon_{I_{\text{d}}} + \omega_0 C_{\text{t}}\epsilon_{V_{\text{q}}} \\ \epsilon_{I_{\text{q}}} - \omega_0 C_{\text{t}}\epsilon_{V_{\text{d}}} \end{bmatrix} - \begin{bmatrix} 0 \\ 0 \\ I_{\text{L,d}}(\boldsymbol{\epsilon}_{\boldsymbol{V}_{\text{dq}}}) \\ I_{\text{L,q}}(\boldsymbol{\epsilon}_{\boldsymbol{V}_{\text{dq}}}) \end{bmatrix}, \quad (37)$$

in PHS form (1). The Hamiltonian of (37) is

$$\begin{aligned} H_{\text{c}}(\boldsymbol{\epsilon}) &= \frac{L_{\text{t}}}{2\nu_{11}}\big(\epsilon_{I_{\text{d}}} + \omega_0 C_{\text{t}}\epsilon_{V_{\text{q}}}\big)^2 + \frac{C_{\text{t}}}{2}\big(\epsilon_{V_{\text{d}}}\big)^2 \\ &\quad + \frac{L_{\text{t}}}{2\nu_{11}}\big(\epsilon_{I_{\text{q}}} - \omega_0 C_{\text{t}}\epsilon_{V_{\text{d}}}\big)^2 + \frac{C_{\text{t}}}{2}\big(\epsilon_{V_{\text{q}}}\big)^2 \end{aligned} \quad (38)$$

and the $\boldsymbol{J}_{\text{c}}$ and $\boldsymbol{R}_{\text{c}}$ matrices remain unchanged from (20). Note that only the load currents $\boldsymbol{I}_{\text{L,dq}}$ influence the error dynamics (37) as discussed in Remark 5.

Proposition 3: The current of a ZP load (cf. (11)) as a function of the voltage error $\boldsymbol{\epsilon}_{\boldsymbol{V}_{\text{dq}}}$ is given in *dq* coordinates by

$$\boldsymbol{I}_{\text{L,dq}}(\boldsymbol{\epsilon}_{\boldsymbol{V}_{\text{dq}}}) = \boldsymbol{I}_{\text{L,dq}}(\boldsymbol{V}_{\text{dq}}) - \boldsymbol{I}_{\text{L,dq}}(\boldsymbol{V}_{\text{dq}}^*), \quad (39)$$

which is approximated by

$$\boldsymbol{I}_{\text{L,dq}}(\boldsymbol{\epsilon}_{\boldsymbol{V}_{\text{dq}}}) \approx \boldsymbol{W}(\boldsymbol{V}_{\text{dq}}^*)\,\boldsymbol{\epsilon}_{\boldsymbol{V}_{\text{dq}}}. \quad (40)$$

For the approximation,

$$\boldsymbol{W}(\boldsymbol{V}_{\text{dq}}^*) = \begin{bmatrix} Z_P & -Z_Q \\ Z_Q & Z_P \end{bmatrix} - \frac{2V_{\text{d}}^* V_{\text{q}}^*}{V^{*2}} \begin{bmatrix} -P_Q & P_P \\ P_P & P_Q \end{bmatrix} - \frac{V_{\text{d}}^{*2} - V_{\text{q}}^{*2}}{V^{*2}} \begin{bmatrix} P_P & P_Q \\ P_Q & P_P \end{bmatrix} \quad (41)$$

is the gradient of the ZP load current at the reference voltage and $V^{*2} = V_{\text{d}}^{*2} + V_{\text{q}}^{*2}$ is the amplitude of the voltage phasor.

Proof: Consider the phasors $V\angle\delta_V$ and $I\angle\delta_I$ of the load relative to the *dq* frame, with the phase difference $\theta = \delta_V - \delta_I$ as depicted in Fig. 3. By projecting $I\angle\delta_I$ onto $V\angle\delta_V$ with a rotation of $-\theta$, we obtain its components parallel $I_{\parallel} = I\cos(-\theta) = I\cos(\theta)$ and perpendicular $I_{\perp} = I\sin(-\theta) = -I\sin(\theta)$ to $V\angle\delta_V$. Using the definition of the instantaneous power of phasors, we get

$$P = VI\cos\theta \Rightarrow I_{\parallel} = \frac{P}{V} \quad (42\text{a})$$

$$Q = VI\sin\theta \Rightarrow I_{\perp} = -\frac{Q}{V} \quad (42\text{b})$$

which may be rotated by δ_V to obtain *dq* coordinates

$$\begin{bmatrix} I_{\text{L,d}} \\ I_{\text{L,q}} \end{bmatrix} = \frac{1}{V} \begin{bmatrix} \cos\delta_V & -\sin\delta_V \\ \sin\delta_V & \cos\delta_V \end{bmatrix} \begin{bmatrix} P \\ Q \end{bmatrix}. \quad (43)$$

Substituting $V^2 = V_{\text{d}}^2 + V_{\text{q}}^2$, $\delta_V = \arctan(V_{\text{q}}/V_{\text{d}})$, and (11) in (43), we get the $\boldsymbol{V}_{\text{dq}}$ dependent current of a ZP load

$$\boldsymbol{I}_{\text{L,dq}}(\boldsymbol{V}_{\text{dq}}) = \begin{bmatrix} Z_P V_{\text{d}} - Z_Q V_{\text{q}} \\ Z_P V_{\text{q}} + Z_Q V_{\text{d}} \end{bmatrix} + \frac{1}{V^2} \begin{bmatrix} P_P V_{\text{d}} - P_Q V_{\text{q}} \\ P_P V_{\text{q}} + P_Q V_{\text{d}} \end{bmatrix} \quad (44)$$

with its first-order Taylor approximation

$$\begin{aligned} \boldsymbol{I}_{\text{L,dq}}(\boldsymbol{\epsilon}_{\boldsymbol{V}_{\text{dq}}}) &\approx \left.\frac{\partial \boldsymbol{I}_{\text{L,dq}}(\boldsymbol{V}_{\text{dq}})}{\partial \boldsymbol{V}_{\text{dq}}}\right|_{\boldsymbol{V}_{\text{dq}}^*} \boldsymbol{\epsilon}_{\boldsymbol{V}_{\text{dq}}} + \boldsymbol{I}_{\text{L,dq}}(\boldsymbol{V}_{\text{dq}})|_{\boldsymbol{V}_{\text{dq}}^*} \\ &\quad - \frac{\partial \boldsymbol{I}_{\text{L,dq}}(\boldsymbol{V}_{\text{dq}}^*)}{\partial \boldsymbol{V}_{\text{dq}}^*}(\boldsymbol{\epsilon}_{\boldsymbol{V}_{\text{dq}}^*}) - \boldsymbol{I}_{\text{L,dq}}(\boldsymbol{V}_{\text{dq}}^*) \end{aligned} \quad (45)$$

at the reference voltage $\boldsymbol{V}_{\text{dq}}^*$, where $\boldsymbol{\epsilon}_{\boldsymbol{V}_{\text{dq}}^*} := \boldsymbol{V}_{\text{dq}}^* - \boldsymbol{V}_{\text{dq}}^* = \boldsymbol{0}$, and the gradient matrix

$$\boldsymbol{W}(\boldsymbol{V}_{\text{dq}}^*) := \left.\frac{\partial \boldsymbol{I}_{\text{L,dq}}(\boldsymbol{V}_{\text{dq}})}{\partial \boldsymbol{V}_{\text{dq}}}\right|_{\boldsymbol{V}_{\text{dq}}^*}. \quad (46)$$

Calculating $\boldsymbol{W}(\boldsymbol{V}_{\text{dq}}^*)$ from (46) yields (41) and (45) simplifies to (40). ∎

Proposition 4: The controlled DGU in (35) with error dynamics (37) is strictly passive and has a globally asymptotically stable equilibrium at any desired voltage reference $V^{*2} = V_{\text{d}}^{*2} + V_{\text{q}}^{*2}$ if

$$\nu_{11} > 0, \quad (47\text{a})$$

$$\alpha_{11} < 0, \quad (47\text{b})$$

$$\alpha_{22} < 0, \quad (47\text{c})$$

$$Z_P V^{*2} > \sqrt{P_P^2 + P_Q^2}. \quad (47\text{d})$$

Proof: The restrictions for strict passivity follow from the requirements in Lemma 1. Since $H_{\text{c}}(\boldsymbol{\epsilon})$ in (38) is convex under (29), (47a) follows from (33) to ensure $\boldsymbol{Q} \succ 0$. Furthermore, we find the damping matrix

$$\boldsymbol{R} = \boldsymbol{R}_c + \boldsymbol{R}_{\text{L}} \quad (48)$$

of the DGU error dynamics (37) by adding the damping effects of the nonlinear load currents $\boldsymbol{I}_{\text{L,dq}}(\boldsymbol{\epsilon}_{\boldsymbol{V}_{\text{dq}}})$ summarized in $\boldsymbol{R}_{\text{L}}$, to that of the undisturbed, linear system in (20). From (40) in Proposition 3, we can find the load current interconnection and damping matrices, $\boldsymbol{J}_{\text{L}}$ and $\boldsymbol{R}_{\text{L}}$, as the symmetric and skew-symmetric parts of (41), respectively:

$$-\boldsymbol{I}_{\text{L,dq}} \approx -\boldsymbol{W}(\boldsymbol{V}_{\text{dq}}^*)\boldsymbol{\epsilon}_{\boldsymbol{V}_{\text{dq}}} =: (\boldsymbol{J}_{\text{L}} - \boldsymbol{R}_{\text{L}})\boldsymbol{\epsilon}_{\boldsymbol{V}_{\text{dq}}}. \quad (49)$$

Note that $\boldsymbol{I}_{\text{L,dq}}$ acts negatively on the voltage error differential equation in (37). With

$$\boldsymbol{R}_{\text{L}} = \frac{\boldsymbol{W}(\boldsymbol{V}_{\text{dq}}^*) + \boldsymbol{W}^{\mathsf{T}}(\boldsymbol{V}_{\text{dq}}^*)}{2}, \quad (50)$$

$$\begin{aligned} &= \begin{bmatrix} Z_P & 0 \\ 0 & Z_P \end{bmatrix} - \frac{2V_{\text{d}}^* V_{\text{q}}^*}{V^{*2}} \begin{bmatrix} -P_Q & P_P \\ P_P & P_Q \end{bmatrix} \\ &\quad - \frac{V_{\text{d}}^{*2} - V_{\text{q}}^{*2}}{V^{*2}} \begin{bmatrix} P_P & P_Q \\ P_Q & P_P \end{bmatrix}, \end{aligned} \quad (51)$$

TABLE I
Electrical Line Parameters

	Positive-sequence	Zero-sequence
Resistance R_{ij} (Ω/km)	0.01273	0.3864
Inductance L_{ij} (mH/km)	0.9337	4.1264
Capacitance C_{ij} (nF/km)	12.74	7.751

TABLE II
Reference Voltages and ZP Load Parameters of the DGUs
(Parameters in Brackets Indicate Values After $t = 3\,$s)

DGU	V_d^*(pu)	V_q^*(pu)	Z_P, P_P (kW)	Z_Q, P_Q (kVAR)
1 (blue)	0.75	0.65	95, 80	23, 20
2 (red)	0.85	0.55	80, 31	0, 9
3 (yellow)	0.9	0.5	46, 38	30, 25
4 (purple)	0.7	0.7	33, 2 (98, 42)	65, 27 (80, 35)
5 (turquoise)	0.8	0.6	40, 20	10, 20

and (20), (48) is given by

$$\boldsymbol{R} = \begin{bmatrix} \mathrm{Diag}\left[-\alpha_{11}, -\alpha_{22}\right] & \boldsymbol{0}_{2\times2} \\ \boldsymbol{0}_{2\times2} & \boldsymbol{R}_\mathrm{L} \end{bmatrix}. \qquad (52)$$

By calculating the eigenvalues of (52),

$$\lambda_1 = -\alpha_{11}, \lambda_2 = -\alpha_{22}, \lambda_{3,4} = Z_P \pm \frac{\sqrt{P_P^2 + P_Q^2}}{V^{*2}}, \quad (53)$$

we obtain (47b), (47c) and (47d) since $\lambda_k > 0$ must hold for all k to give $\boldsymbol{R} \succ 0$. Under (47), we therefore fulfill the requirements for Lemma 1 from which strict passivity and global asymptotic stability of the equilibrium at the desired voltage reference V^* follows. ∎

With the strict passivity of the controlled DGUs assured by Proposition 4, the global asymptotic voltage and frequency stability of the microgrid exemplified in Fig. 1 follows directly from Proposition 2 and Remark 4.

V. Simulation

In this section, we show the viability of the local VSI P-controller in (34) as well as the performance attained by simulation in Matlab/Simulink. For this, we use the islanded microgrid in Fig. 1 comprising five DGUs connected by π-model lines. Each DGU comprises a VSI, a filter and a ZP load (cf. Fig. 2). All DGU filters are parameterized identically with $R_{ti} = 0.1\,\Omega$, $L_{ti} = 100\,\mu$H, $C_{ti} = 62.86\,\mu$F. The default Matlab per-kilometer values are used for the three-phase lines (see Table I) with lengths as given in Fig. 1. To investigate the robustness of the controllers, in contrast to the control design model, a zero-sequence is included in the simulation. Furthermore, the control parameters are chosen to $\alpha_{11} = \alpha_{22} = -10^{-6}$ and $\nu_{11} = 1$. The reference voltage of the DGUs are arbitrarily set with $V_{amplitude} = 325\,$V $(1\,$pu$)$ and the load parameters are arbitrarily chosen to satisfy (47d) (cf. Table II). The simulation starts off with DGU 5 disconnected from the microgrid. To test the feasibility of a plug-and-play operation, DGU 5 is connected at

(a) V_d components at the PCCs   (b) V_q components at the PCCs

(c) THD of the phase a voltages at the PCCs   (d) Voltage frequencies at the PCCs
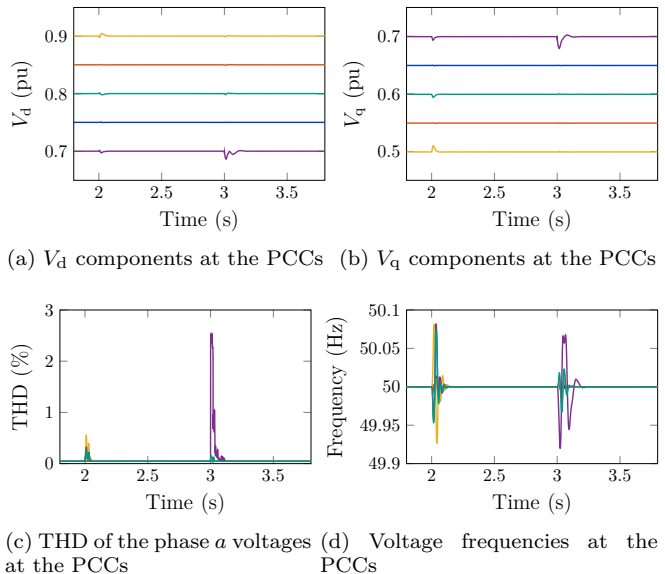
Fig. 4. Simulation results of the local P-controllers; DGU colors are given in Table II

$t = 2\,$s as indicated in Fig. 1. To test the robustness of the microgrid, an additional load is connected to DGU 4 (cf. Table II) at $t = 3\,$s. The results in Fig. 4 indicate only small deviations from the dq references when the system is disturbed. Furthermore, the total harmonic distortion (THD) remains below 3 % despite the disturbances and changes in the microgrid. The frequencies at the PCCs of the DGUs remain within a 0.1 Hz band around the nominal frequency of 50 Hz. These results compare favorably to the IEEE 1159-2009 restrictions [23] of THDs less than 5 % and frequency variations smaller than 0.2 Hz.

VI. Conclusion

In this paper, we presented a new approach for the decentralized scalable, plug-and-play voltage and frequency stabilization of islanded inverter-based AC microgrids on the basis of a systematic IDA-PBC design. By following the port-Hamiltonian paradigm, we directly obtain a Lyapunov function used for a subsequent stability analysis and obviate its possibly cumbersome proposition. Under inequality conditions obtained from analyzing ZP load dynamics, we prove global asymptotic voltage and frequency stability. An extension to ZIP and exponential loads using the proposed procedure is possible as will be shown in future contributions.

References

[1] J. Schiffer, D. Zonetti, R. Ortega, A. M. Stanković, T. Sezi, and J. Raisch. "A survey on modeling of microgrids—From fundamental physics to phasors and voltage sources". In: *Automatica* 74 (2016), pp. 135–150.

[2] J. M. Guerrero, J. C. Vasquez, J. Matas, L. G. de Vicuna, and M. Castilla. "Hierarchical Control of Droop-Controlled AC and DC Microgrids—A General Approach Toward Standardization". In: *IEEE Transactions on Industrial Electronics* 58 (2011), pp. 158–172.

[3] J. M. Guerrero, M. Chandorkar, T. Lee, and P. C. Loh. "Advanced Control Architectures for Intelligent Microgrids—Part I: Decentralized and Hierarchical Control". In: *IEEE Transactions on Industrial Electronics* 60 (2013), pp. 1254–1262.

[4] D. E. Olivares, A. Mehrizi-Sani, A. H. Etemadi, C. A. Cañizares, R. Iravani, M. Kazerani, A. H. Hajimiragha, O. Gomis-Bellmunt, M. Saeedifard, R. Palma-Behnke, G. Jimeénez-Estévez, and N. D. Hatziargyriou. "Trends in Microgrid Control". In: *IEEE Transactions on Smart Grid* 5 (2014), pp. 1905–1919.

[5] M. S. Sadabadi, Q. Shafiee, and A. Karimi. "Plug-and-Play Voltage Stabilization in Inverter-Interfaced Microgrids via a Robust Control Strategy". In: *IEEE Transactions on Control Systems Technology* 25 (2017), pp. 781–791.

[6] L. Meng, Q. Shafiee, G. Ferrari-Trecate, H. Karimi, D. Fulwani, X. Lu, and J. M. Guerrero. "Review on Control of DC Microgrids and Multiple Microgrid Clusters". In: *IEEE Journal of Emerging and Selected Topics in Power Electronics* 5 (2017), pp. 928–948.

[7] F. Dörfler, J. W. Simpson-Porco, and F. Bullo. "Plug-and-Play Control and Optimization in Microgrids". In: *53rd IEEE Conference on Decision and Control*. Los Angeles, California, USA, 2014, pp. 211–216.

[8] S. Riverso, F. Sarzo, and G. Ferrari-Trecate. "Plug-and-Play Voltage and Frequency Control of Islanded Microgrids With Meshed Topology". In: *IEEE Transactions on Smart Grid* 6 (2015), pp. 1176–1184.

[9] M. Tucci, A. Floriduz, S. Riverso, and G. Ferrari-Trecate. "Plug-and-play control of AC islanded microgrids with general topology". In: *2016 European Control Conference*. Aalborg, Denmark, 2016, pp. 1493–1500.

[10] A. Floriduz, M. Tucci, S. Riverso, and G. Ferrari-Trecate. "Approximate Kron Reduction Methods for Electrical Networks With Applications to Plug-and-Play Control of AC Islanded Microgrids". In: *IEEE Transactions on Control Systems Technology* (2018). early access, pp. 1–14.

[11] M. Tucci and G. Ferrari-Trecate. "Voltage and frequency control in AC islanded microgrids: a scalable, line-independent design algorithm". In: *IFAC-PapersOnLine* 50 (2017). 20th IFAC World Congress, pp. 13922–13927.

[12] P. Nahata, R. Soloperto, M. Tucci, A. Martinelli, and G. Ferrari-Trecate. "A Passivity-Based Approach to Voltage Stabilization in DC Microgrids with ZIP loads". In: *Automatica, submitted* (2018). URL: http://infoscience.epfl.ch/record/253266.

[13] R. Sepulchre, M. Janković, and P. Kokotović. *Constructive Nonlinear Control*. Springer London, 1997.

[14] F. M. Serra, C. H. D. Angelo, and D. G. Forchetti. "Interconnection and damping assignment control of a three-phase front end converter". In: *International Journal of Electrical Power & Energy Systems* 60 (2014), pp. 317–324.

[15] F. M. Serra and C. H. D. Angelo. "IDA-PBC controller design for grid connected Front End Converters under non-ideal grid conditions". In: *Electric Power Systems Research* 142 (2017), pp. 12–19.

[16] F. M. Serra, C. H. D. Angelo, and D. G. Forchetti. "IDA-PBC control of a DC–AC converter for sinusoidal three-phase voltage generation". In: *International Journal of Electronics* 104 (2017), pp. 93–110.

[17] V. Duindam, A. Macchelli, S. Stramigioli, and H. Bruyninckx. *Modeling and Control of Complex Physical Systems*. Springer Berlin Heidelberg, 2009.

[18] P. Kotyczka. "Local linear dynamics assignment in IDA-PBC". In: *Automatica* 49 (2013), pp. 1037–1044.

[19] R. Ortega and E. García-Canseco. "Interconnection and Damping Assignment Passivity-Based Control: A Survey". In: *European Journal of Control* 10 (2004), pp. 432 –450.

[20] H. K. Khalil. *Nonlinear systems*. 3rd ed. Prentice-Hall, 2002.

[21] A. van der Schaft. *L2 Gain and Passivity Techniques in Nonlinear Control*. Springer International Publishing AG, 2017.

[22] J. Machowski, J. W. Bialek, and J. R. Bumby. *Power System Dynamics: Stability and Control*. Chichester: John Wiley & Sons, Ltd, 2012.

[23] "IEEE Recommended Practice for Monitoring Electric Power Quality". In: *IEEE Std 1159-2009* (2009), pp. c1–81.